Autophagy
Publication details, including instructions for authors and subscription information:
http://www.tandfonline.com/loi/kaup20

Mutations in the ubiquitin-binding domain of OPTN/optineurin interfere with autophagy-mediated degradation of misfolded proteins by a dominant-negative mechanism

Wen-Chuan Shen[ab], Huei-Ying Li[b], Guang-Chao Chen[c], Yijuang Chern[ab] & Pang-hsien Tu[ab]

[a] Taiwan International Graduate Program in Molecular Medicine; National Yang-Ming University and Academia Sinica; Taipei, Taiwan

[b] Institute of Biomedical Sciences; Academia Sinica; Taipei, Taiwan

[c] Institute of Biological Chemistry; Academia Sinica; Taipei, Taiwan

Accepted author version posted online: 27 Apr 2015.

To cite this article: Wen-Chuan Shen, Huei-Ying Li, Guang-Chao Chen, Yijuang Chern & Pang-hsien Tu (2015) Mutations in the ubiquitin-binding domain of OPTN/optineurin interfere with autophagy-mediated degradation of misfolded proteins by a dominant-negative mechanism, Autophagy, 11:4, 685-700, DOI: 10.4161/auto.36098

To link to this article: http://dx.doi.org/10.4161/auto.36098

BASIC RESEARCH PAPER

Autophagy 11:4, 685–700; April 2015; © 2015 Taylor & Francis Group, LLC

Mutations in the ubiquitin-binding domain of OPTN/optineurin interfere with autophagy-mediated degradation of misfolded proteins by a dominant-negative mechanism

Wen-Chuan Shen,[1,2] Huei-Ying Li,[2] Guang-Chao Chen,[3] Yijuang Chern,[1,2] and Pang-hsien Tu[1,2,*]

[1]Taiwan International Graduate Program in Molecular Medicine; National Yang-Ming University and Academia Sinica; Taipei, Taiwan; [2]Institute of Biomedical Sciences; Academia Sinica; Taipei, Taiwan; [3]Institute of Biological Chemistry; Academia Sinica; Taipei, Taiwan

Keywords: optineurin, autophagy, huntingtin, TARDBP/TDP-43, dominant-negative

Abbreviations: Ab, antibody; ALS, amyotrophic lateral sclerosis; BafA1, bafilomycin A_1; CCD, coiled-coil domain; E_f, FRET efficiency; FT, filter-trap assay; HD, Huntington disease; IBs, inclusion bodies; IP, immunoprecipitation; K48, lysine 48; K63, lysine 63; LIR, LC3-interacting region; mHTT, mutant huntingtin; MYO6, myosin VI; OPTN, optineurin; PBS, phosphate-buffered saline; PFA, paraformaldehyde; TARDBP/TDP-43, TAR DNA-binding protein; TBK1, TANK-binding kinase 1; TUBA, alpha tubulin; Ub, ubiquitin B/C/D; UbBD, ubiquitin-binding domain; UPS, ubiquitin-proteasome system; WB, western blot; WT, wild type.

OPTN (optineurin) is an autophagy receptor and mutations in the *OPTN* gene result in familial glaucoma (E50K) and amyotrophic lateral sclerosis (ALS) (E478G). However, the mechanisms through which mutant OPTN leads to human diseases remain to be characterized. Here, we demonstrated that OPTN colocalized with inclusion bodies (IBs) formed by mutant HTT/huntingtin protein (mHTT) in R6/2 transgenic mice and IBs formed by 81QNmHTT (nuclear form), 109QmHTT (cytoplasmic form) or the truncated form of TARDBP/TDP-43 ($TARDBP^{ND251}$) in Neuro2A cells. This colocalization required the ubiquitin (Ub)-binding domain (UbBD, amino acids 424 to 511) of OPTN. Overexpression of wild-type (WT) OPTN decreased IBs through K63-linked polyubiquitin-mediated autophagy. E50K or 210 to 410Δ (with amino acids 210 to 410 deleted) whose mutation or deletion was outside the UbBD decreased the IBs formed by 109QmHTT or $TARDBP^{ND251}$, as was the case with WT OPTN. In contrast, UbBD mutants, including E478G, D474N, UbBDΔ, 411 to 520Δ and 210 to 520Δ, increased accumulation of IBs. UbBD mutants (E478G, UbBDΔ) retained a substantial ability to interact with WT OPTN, and were found to colocalize with polyubiquitinated IBs, which might occur indirectly through their WT partner in a WT-mutant complex. They decreased autophagic flux evidenced by alteration in LC3 level and turnover and in the number of LC3-positive puncta under stresses like starvation or formation of IBs. UbBD mutants exhibited a weakened interaction with MYO6 (myosin VI) and TOM1 (target of myb1 homolog [chicken]), important for autophagosome maturation, in cells or sorted 109QmHtt IBs. Taken together, our data indicated that UbBD mutants acted as dominant-negative traps through the formation of WT-mutant hybrid complexes to compromise the maturation of autophagosomes, which in turn interfered with OPTN-mediated autophagy and clearance of IBs.

Introduction

Neurodegenerative diseases such as Alzheimer, Parkinson, amyotrophic lateral sclerosis (ALS), and Huntington (HD) are heterogeneous in etiology and clinical presentation, but are dubbed as protein-misfolding diseases, as they share the presence of signature inclusion bodies (IBs) in affected nervous tissue.[1] For instance, HD is caused by an abnormal expansion of the CAG repeat in the *HTT* gene encoding mutant huntingtin (mHTT), which forms IBs in nuclei as well as neurites of neurons. ALS, sporadic and familial alike, also develops hallmark IBs formed by TARDBP in spinal cord motoneurons.[2-4] The ubiquitin-proteasome system (UPS) and autophagy play an essential role in removing misfolded IBs in these neurodegenerative diseases.[5,6] Recent studies reveal that ubiquitin-selective autophagy requires adaptors to recognize the polyubiquitin chain on the autophagy substrates to direct them for degradation through interaction with the autophagosome marker MAP1LC3/LC3 (microtubule-associated protein 1 light chain 3).[5,7,8] Several autophagy receptors, which contain both ubiquitin-

*Correspondence to: Pang-hsien Tu; Email: btu@ibms.sinica.edu.tw
Submitted: 10/30/2013; Revised: 08/08/2014; Accepted: 08/15/2014
http://dx.doi.org/10.4161/auto.36098

binding domain (UbBD) and LC3-interacting region (LIR), have been identified, including SQSTM1/p62,[9] the prototype adaptor, NBR1,[10] and CALCOCO2/NDP52.[11] All of these autophagy receptors identified so far exhibit a preference to the Lysine 63 (K63)-linked ubiquitin signal, which has been associated with IBs of various neurodegenerative diseases aforementioned.[5,7,8,12-15]

OPTN has recently been reported as a novel autophagy receptor, which can inhibit the growth of *Salmonella* by autophagy. The interaction of OPTN with LC3A/B (hereafter LC3) is enhanced by its phosphorylation by TBK1 (TANK-binding kinase 1) at the LIR motif.[16] In addition, OPTN also drives autophagosome maturation by fusion with endosomes by interacting with myosin VI.[17] Unlike other autophagy receptors, which are degraded by autophagy, OPTN is normally degraded by the proteasome pathway. The importance of OPTN in neurodegenerative diseases has been fully established only after the identification of mutations in the *OPTN* gene, in familial ALS patients.[18] Since then, OPTN has been shown to colocalize with the IBs of various neurodegenerative diseases, including Alzheimer, Parkinson, ALS, and HD.[18-21] A study demonstrates that lower expression level of OPTN may account for the selective vulnerability of medium spiny neurons of striatum in HD.[22] In addition, OPTN may promote neuronal survival by counteracting the glutamate-induced neurotoxicity in diseases.[23,24] These results demonstrate that OPTN is neuroprotective. Despite these progresses, the pathogenic mechanisms by which mutant OPTN protein causes diseases remain to be elucidated. A recent study indicates that OPTN mediates autophagy activity through an undefined Ub-independent mechanism to clear IBs.[25] In this study, we demonstrated that OPTN harboring mutations in the ubiquitin-binding domain interfered with the autophagy process and autophagy-mediated clearance of IBs in a dominant-negative fashion.

Results

Colocalization of OPTN with IBs through its ubiquitin-binding domain

To validate the role that OPTN plays in neurodegenerative diseases, we examined the distribution pattern of OPTN in the HD mouse model R6/2 transgenic mice. Consistent with the recent study from HD patients,[19] confocal microscopy analyses showed that OPTN signal was primarily, if not exclusively, colocalized with that of mHTT IBs (EM48) and ubiquitin in both the nucleus and cytoplasm of neurons from cortex and striatum (**Fig. 1A**). Similarly, OPTN was also found within the ubiquitinated mHTT IBs in Neuro2A cells, which expressed the cytoplasmic form (109Q) or the nuclear form (81QN) of eGFP-tagged mHTT (**Fig. 1B**). In addition, OPTN was also colocalized with the IBs formed by the eGFP-TARDBP^{ND251} (TARDBP^{ND251}), a truncated form of TARDBP with the N-terminal 251 amino acids deleted, which recapitulated cardinal features of IBs found in ALS (**Fig. 1C**).[26] To further characterize this, we isolated these IBs with high purity using a cell sorter as previously described (**Fig. S1**).[26] Western blot analysis confirmed the association of OPTN with these IBs in the P1 or IB fraction (**Fig. 1D**).

OPTN is composed of multiple functional domains defined by the ability to interact with partner proteins involved in trafficking, such as the RAB8-interacting domain (58 to 209), MYO6-interacting domain (412 to 520), and UbBD (424 to 511).[27,28] To identify the region responsible for the colocalization of OPTN with protein aggregates, various truncated forms of OPTN constructs were generated (**Fig. 1E**) and tested for their ability to colocalize with IBs (**Fig. 1F, 1G**). As expected, almost all (97%) of the mHTT IBs contained the wild-type (WT) OPTN, and a comparable level of colocalization (92%) was also observed between mHTT IBs and 210 to 410Δ OPTN with amino acids 210 to 410 deleted. In contrast, a high level of 210 to 520Δ, 411 to 520Δ or UbBDΔ OPTN was detected in ~23%, 25%, and 29% of mHTT IBs, respectively, although the majority of IBs contained low level of these proteins. These data indicated the UbBD to be the region primarily responsible for the colocalization of OPTN with misfolded IBs.

We next examined the effect of OPTN with mutations in different domains on the colocalization with mHTT IBs. The E50K mutation, which was outside of the UbBD, had no detectable impact (97%); the E478G and D474N mutations, which were located within the UbBD, decreased colocalization by 32% and 26%, respectively (**Fig. 1F, 1G**). Similarly, WT and E50K were found in the majority of TARDBP^{ND251} IBs, but the UbBDΔ and E478G had lower colocalization rates (**Fig. S2**). These results showed that mutations and deletions involving the UbBD affected the OPTN interaction with IBs.

OPTN reduces mHTT IBs through autophagy

We then investigated the effect of OPTN on clearance of mHTT IBs by filter-trap assay, which detected the IB fraction of mHTT. Overexpression of WT OPTN reduced IBs formed by either 109Q or 81QN mHTT (**Fig. 2A**); *Optn* depletion by shRNA complementarily increased the levels of mHTT aggregates (**Fig. 2B**). The OPTN-mediated reduction in mHTT IBs was blocked by autophagy inhibitors, 3-methyladenine (3MA) and bafilomycin A_1 (BafA1) (**Fig. 2C**); in contrast, the ubiquitin-proteasomal system (UPS) inhibitor MG132 failed to exhibit any significant effect.

For further analysis, we examined the impact on the OPTN-mediated decrease in the 109QmHTT IBs through a genetics approach. The cell lysate was separated into RIPA-soluble or non-IB (S) and RIPA-insoluble or IB (I) fraction. Consistently, overexpression of WT OPTN decreased the level of 109QmHTT in the IB (I) fraction (asterisk) on western blot (**Fig. 2D**), and the corresponding insolubility index of 109QmHTT by 50%. The effect of WT OPTN was blocked by *Atg5* knockdown in Neuro2A cells (**Fig. 2D**) and in *Atg5*-null mouse embryonic fibroblasts (MEFs) as well (**Fig. 2E**). As expected, overexpression of the LIR-mutant OPTN, F178A, or LIRΔ, failed to reduce the level of insoluble 109QmHTT and the insolubility index as WT OPTN did (**Fig. 2F**). Moreover, in Neuro2A cells depleted of *Optn* by shRNA,

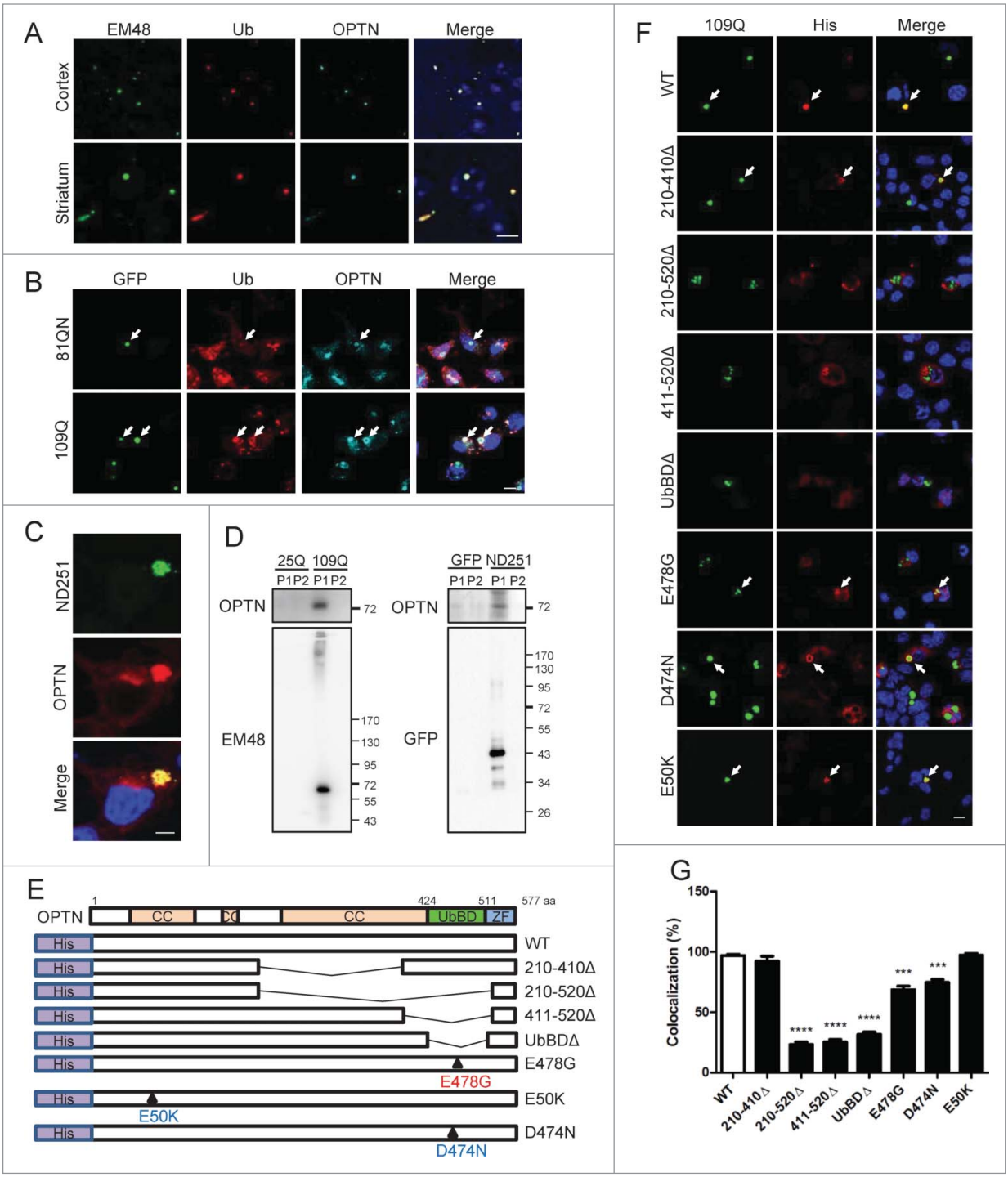

Figure 1. Colocalization of OPTN with IBs through UbBD. (**A**) Immunofluorescent confocal images of cortical and striatal sections of the 12-wk-old R6/2 transgenic mice stained with EM48 (mHTT), anti-ubiquitin (Ub) and anti-OPTN antibodies (Abs). (**B**) Confocal images of Neuro2A cells expressing GFP-81QNmHTT or GFP-109QmHTT stained with anti-Ub or anti-OPTN Abs. Arrows show IBs with signals. (**C**) Images of Neuro2A cells expressing eGFP-TARDBP^{ND251} (ND251) stained with anti-OPTN Ab. (**D**) Western blot of the sorted GFP, GFP-positive 25QHTT, 109QmHTT or ND251 particles from IBs (P1) or non-IB (P2) fraction of the Neuro2A cells probed with anti-OPTN, EM48 or GFP Abs. Endogenous OPTN was detected only in 109QmHTT and ND251 IBs. (**E**) Schematic illustration of wild-type (WT) and truncated or mutated OPTN constructs. (**F**) Confocal images of Neuro2A cells co-overexpressing 109QmHTT and OPTN variants as indicated. (**G**) Quantitative graph of colocalization of the OPTN variants with 109QmHTT IBs. ***$P < 0.001$, ****$P < 0.0001$. Scale bar: 5 μm. At least 100 randomly chosen aggregates were calculated in triplicate experiments.

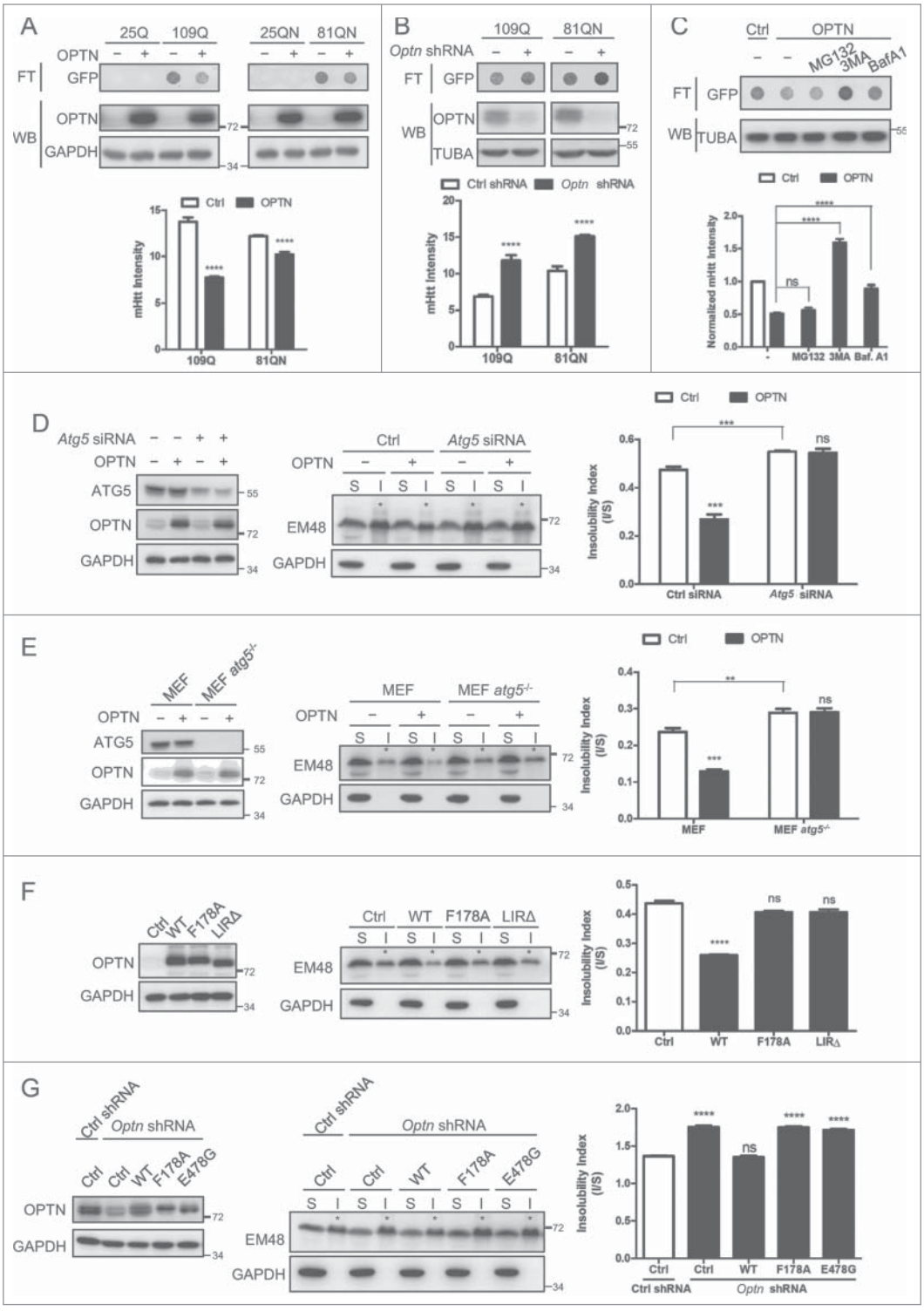

Figure 2. OPTN reduces mHTT IBs through autophagy. (**A**) Filter trap (FT) assay for IBs of Neuro2A cells coexpressing vector or OPTN with 25QHTT (cytoplasmic), 25QNHTT (nuclear), 109QmHTT (cytoplasmic) or 81QNmHTT (nuclear). The corresponding western blotting (WB) showed equal expression of OPTN and loading (GAPDH). Quantitative graph (below) showing OPTN overexpression reduced both 109Q and 81QN IBs. (**B**) FT assay of Neuro2A cells with OPTN knockdown (KD) which increased IBs of both mHTT. TUBA, alpha-tubulin. (**C**) FT assay to show that OPTN-mediated reduction in the 109QmHTT IBs was blocked by 5 mM 3-methyladenine (3MA) or 2 μM bafilomycin A_1 (BafA1), but not by 1 μM MG132. (**D**) Western blot analysis and quantification of the soluble (S, non-IB) and insoluble (I, IB) fractions of Neuro2A cells transfected with constructs as indicated. Please note knockdown of *Atg5* by siRNA blocked the OPTN-mediated reduction in insoluble 109QmHTT (asterisks). (**E**) Similar experiments were conducted in MEF and *Atg5*-null MEF (*atg5*$^{-/-}$) cells. (**F**) Western blot analysis and quantification showed that the LIR mutant, F178A or LIRΔ, had no significant effect on insolubility of mHTT compared with WT OPTN. (**G**) Functional rescue assays of WT and mutant OPTN in Neuro2A cells with knockdown of endogenous *Optn* by shRNA. The left subpanel indicates expression of WT and mutant OPTN. F178A or E478G failed to rescue the defect of OPTN knockdown as WT. All quantified data were collected from 3 independently performed experiments. $^{**}P < 0.01$, $^{***}P < 0.001$, $^{****}P < 0.0001$, ns: not significant.

expression of WT OPTN could restore the ability to decrease insoluble 109QmHTT, but F178A or E478G failed to rescue the defect (**Fig. 2G**), consistent with previous studies.[16,25] These results indicated that the interaction between LC3 and OPTN is important for the clearance of mHTT IBs, and OPTN-mediated degradation of mHTT IBs primarily through autophagy machinery.

OPTN-mediated 109QmHTT reduction occurs preferentially through polyUbK63

Autophagy is reported to primarily target K63-polyubiquitinated (polyUbK63) substrates.[5,8,14] In R6/2 mice, OPTN-positive mHTT IBs in cortex and striatum were labeled by both anti-UbK63- and anti-UbK48-specific antibodies (**Fig. 3A**). To

examine if OPTN-mediated IB degradation through polyUbK63-linked pathway, we compared the effect of ubiquitin (UBB/C/D, hereafter ubiquitin [Ub]), the ubiquitin with K48R mutation (Ub^{K48R}) and the ubiquitin with K63R mutation (Ub^{K63R}) on OPTN-mediated decrease in 109QmHTT IBs in the presence of MG132 to remove potential compounding factors from UPS. Overexpression of WT OPTN alone or together with Ub resulted in a decrease in the insoluble or IB fraction (I) of 109QmHTT. Coexpression of mutant Ub^{K48R} had no discernible effect on OPTN-mediated decrease in insoluble mHTT; in contrast, The Ub^{K63R} mutant blocked the function of OPTN (**Fig. 3B**). To further validate this, the polyUbK48 or polyUbK63 peptide chain was used as a decoy substrate to compete with the 109QmHTT IBs. As shown in Fig. 3C, the polyUbK48 or polyUbK63 chain alone did not exert significant impact on the aggregation of 109QmHTT. However, the polyUbK63 chain inhibited the OPTN-mediated reduction of 109QmHTT IBs in a dose-dependent fashion compared with the polyUbK48 at every dosage (**Fig. 3C**). Together, OPTN preferentially recognized the polyUbK63 signal on its autophagy-mediated degradation substrates such as109QmHTT.

Increase in 109QmHTT IBs by OPTN mutations involving UbBD

We next explored the effect of OPTN mutations on OPTN-dependent degradation of mHTT IBs. As shown in Fig. 4A, mutant OPTN with the mutation site outside of the UbBD, such as 210 to 410Δ or E50K, behaved as WT OPTN, and decreased the insoluble 109QmHTT; however, mutant OPTN with the UbBD deleted, such as 210 to 520Δ, 411 to 520Δ and UbBDΔ, or mutated, such as E478G and D474N, increased the insoluble 109QmHTT by western blot analysis. The increase by OPTN with a mutated or deleted UbBD, could not be blocked by treatment with the autophagy activator rapamycin (**Fig. 4B**). Analysis of the details of the IBs using high content approach revealed that OPTN with a mutated or deleted UbBD, such as 210 to 520Δ, 411 to 520Δ, UbBDΔ, E478G, and D474N, all resulted in an increase in 1) the number of cells containing IBs, 2) the number of aggregates per mm^2 and 3) the average size of individual aggregates, in contrast with the WT, 210 to 410Δ and E50K (**Fig. 4C to F**). Similarly, the WT and E50K decreased, but UbBDΔ, E478G, and D474N increased the number of cells with $TARDBP^{ND251}$ IBs (**Fig. S3A**), and knockdown of OPTN led to an increase in the IBs (**Fig. S3B**).

In addition, the percentage of 109QmHTT particles in P1 (IB), P2 (soluble or monomer) and P5 (intermediate) fractions of Neuro2A cells coexpressing WT or various mutant forms of OPTN was quantified using a cell sorter (**Fig. S1**). As shown in Table 1, the percentage of 109QmHTT particles in the P1 or IB fraction was consistently lower in the presence of WT and E50K, compared with control, but was consistently higher with expression of UbBDΔ or E478G. Together, the results obtained from 3 different approaches all showed that mutant OPTN with dysfunctional UbBD increased the accumulation of 109QmHTT IBs.

Dominant-negative effect on degradation of mHTT IBs by UbBD mutants

Overexpression of UbBD mutants increased the IBs formed by misfolded proteins as knocking down OPTN. Given the evidence that OPTN forms homo-hexamer,[29] we hypothesized that the UbBD-mutated OPTN increased 109QmHTT IBs through a dominant-negative mechanism by interfering with endogenous OPTN. To address this, we first examined if these mutants maintained their ability to interact with WT OPTN. Confocal images showed that tagRFP-WT OPTN colocalized with His-tagged OPTN mutants (**Fig. S4A**). To further analyze this, we generated Cerulean (Ce)-tagged WT OPTN (donor) or Venus (Ve)-tagged WT and various mutant OPTNs (acceptors) for the Acceptor Photobleaching Fluorescence Resonance Energy Transfer (apFRET) studies. High FRET efficiency (E_f) was detected in positive control of the Ce-Ve fusion protein (21.32%), but not or weakly in various negative control combinations, validating the feasibility of this technique (**Fig. S4B**). The E_f of Ce-WT in cells expressing Venus control was 5.87%; when coupled with Ve-WT, Ve-UbBDΔ, Ve-E478G, or Ve-E50K, the E_f increased to 28.76%, 22.36%, 25.37%, and 32.02%, respectively. These results further supported the proposition that WT OPTN not only interacted with WT form, but also with OPTN mutants, UbBDΔ, E478G, and E50K (**Fig. 5A and Fig. S4C**). Next, the immunoprecipitation studies demonstrated that E478G and UbBDΔ could interact with WT OPTN, but with weaker strength compared with the WT or E50K mutant (**Fig. 5B**). In addition, the isolated 109QmHTT IBs also contained a substantial amount of the UbBDΔ or E478G mutant (**Fig. 5C**). Altogether, these data demonstrated the retained capability of the UbBD-mutant OPTN to interact and form hybrid oligomers or complex with the WT counterpart.

We next assessed the inhibition of WT OPTN function as opposed to increasing amount of UbBD-mutated OPTN. As shown in **Fig. 5**D, coexpression of E50K did not interfere with the OPTN-mediated decrease in the insoluble 109QmHTT. In contrast, increases in UbBD-mutant UbBDΔ (**Fig. 5E and Fig. S5**) or E478G (**Fig. 5F and Fig. S5**) gradually effaced WT OPTN of its ability to decrease the insoluble pool of 109QmHTT. These results substantiated the hypothesis that UbBD-mutated OPTN blocked the effect of WT OPTN through a dominant-negative mechanism.

Decreased autophagic flux by UbBD-mutated OPTN

Since UbBD mutants interfered with the ability to reduce misfolded IBs, we explored the impact of these mutants on the autophagy process. As shown in **Fig. 6A and 6B**, under fed conditions with or without BafA1, no clear difference as a group was observed between UbBD mutants (UbBDΔ and E478G) and non-UbBD OPTN (WT and E50K). Under starvation, the LC3-II level increased across all OPTN groups, as expected for increased autophagy activity. However, the WT and E50K samples had significantly lower, but UbBDΔ and E478G samples had higher, LC3-II levels compared with the control.

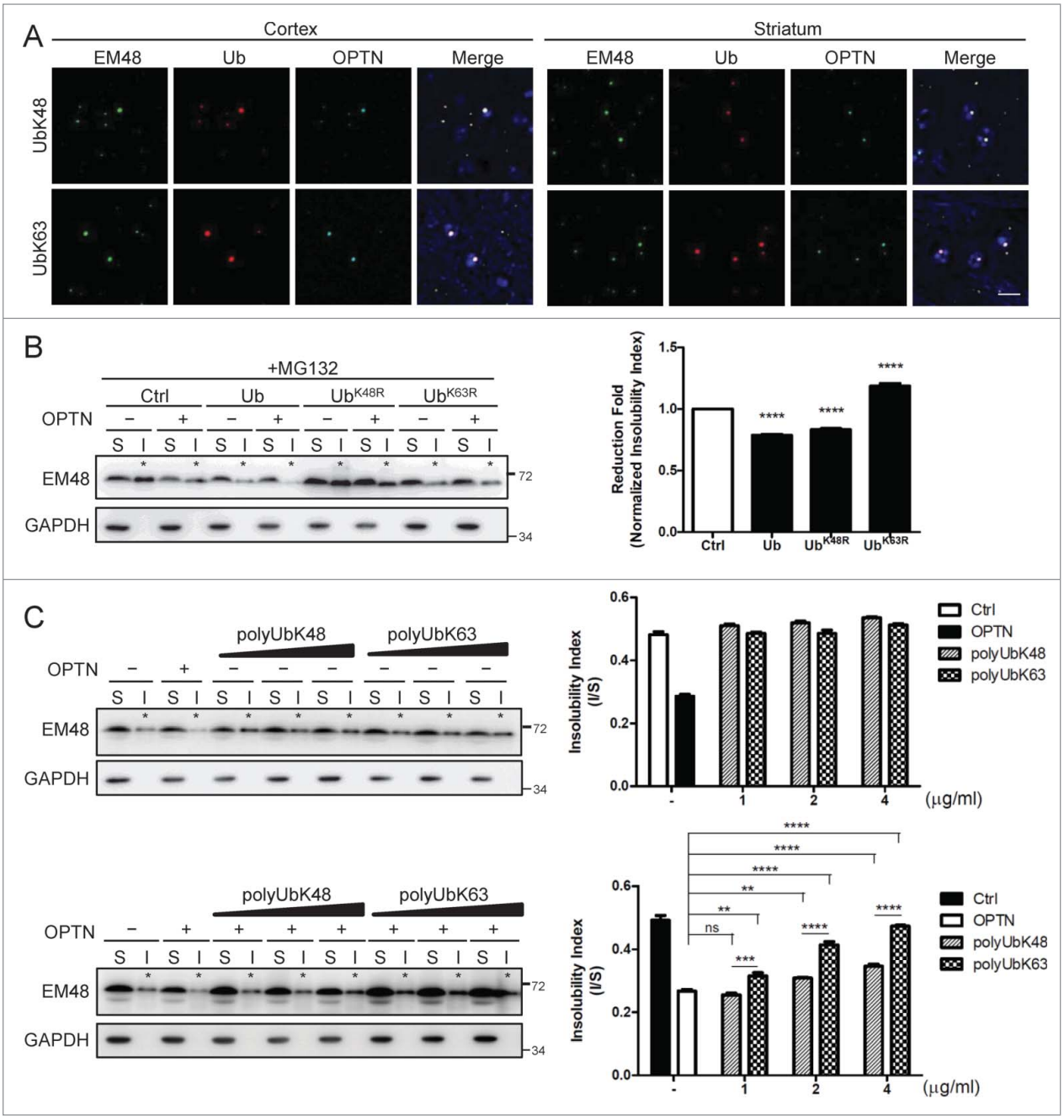

Figure 3. OPTN-mediated 109QmHTT reduction occurs preferentially through polyK63Ub. (**A**) Confocal images of sections of cortex or striatum of 12-wk-old R6/2 mice stained with EM48, anti-OPTN, anti-UbK48- (UbK48) or anti-UbK63-specific (UbK63) Abs. Scale bar: 10 μm. (**B**) Western blot of Neuro2A cells coexpressing 109QmHTT, vector or OPTN plus the UbK48R or UbK63R mutant as indicated, and treated with 1 μM MG132 for 16 h. The reduction fold was calculated first with the insolubility index of the OPTN+ sample normalized with the corresponding OPTN- control. Then the Ub with OPTN or Ub mutant with OPTN sample was again normalized with Ctrl with OPTN (set as 1). The UbK63R mutant blocked the effect of OPTN. (**C**) Western blot of Neuro2A cells coexpressing 109QmHTT with vector (upper panel) or OPTN (lower panel), and treated with polyUbK48 or polyUbK63 peptide chain at 1, 2, or 4 μg/ml (left). The effect of OPTN was compromised by polyUbK63 more significantly than by polyUbK48. The corresponding expression of transfected protein for (**B**) and (**C**) is shown in **Fig. S10A and S10B**. Asterisks on the blots indicate the insoluble fractions. $^{**}P < 0.01$, $^{***}P < 0.001$, $^{****}P < 0.0001$, ns: not significant. All quantified data were collected from 3 independently performed experiments.

Interestingly, with the addition of BafA1 to block fusion of autophagosomes with lysosomes, the change in LC3-II level was in the opposite direction. It became higher with WT and E50K overexpression, but lower with UbBD mutant overexpressions (**Fig. 6B**). The differential effect was better illustrated in light of the LC3-II fold change of starvation over FED (**Fig. 6C**). The increase in LC3-II level by UbBD mutants could be caused by either enhanced formation of autophagosomes or decreased

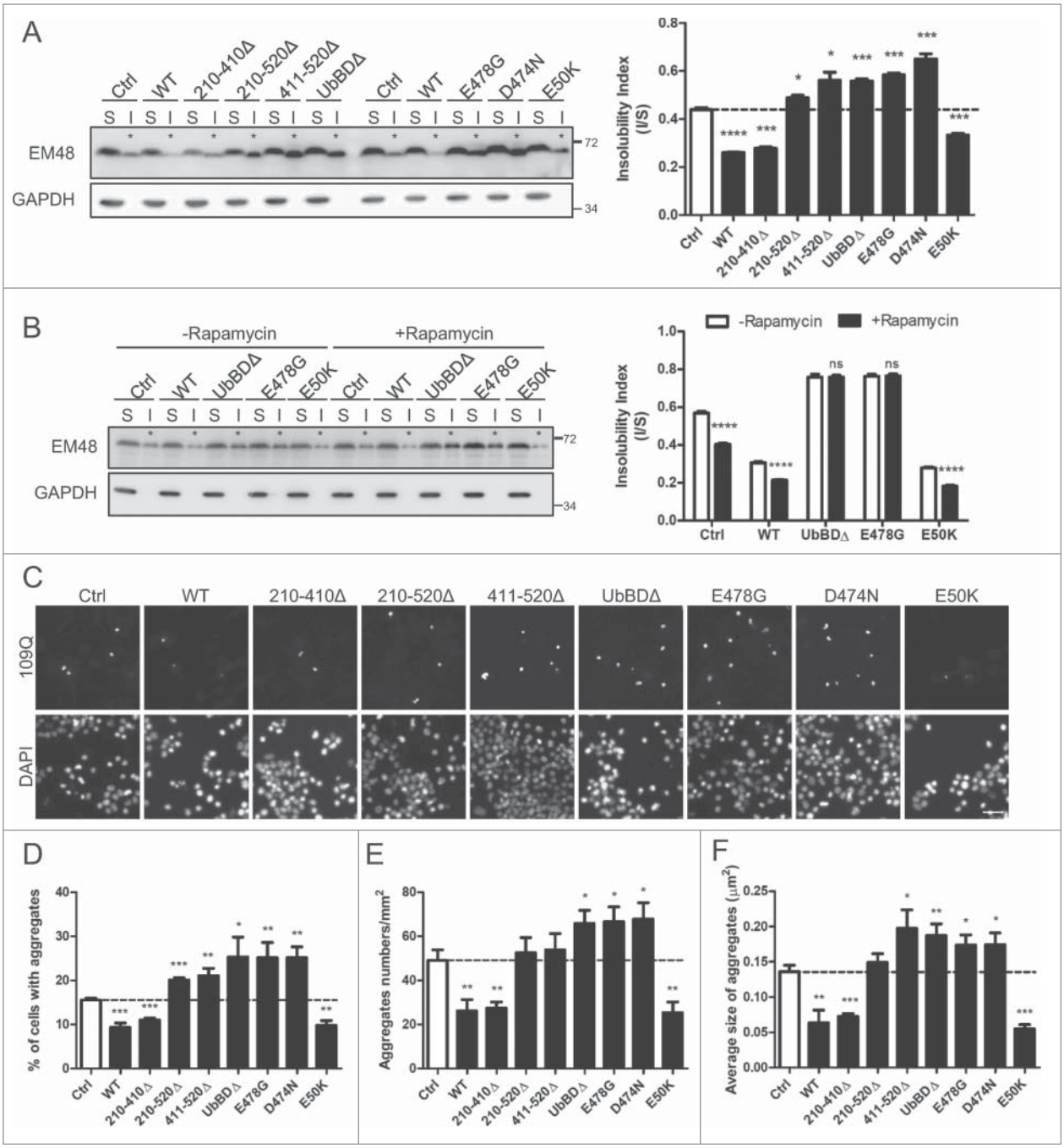

Figure 4. Block of the OPTN-mediated decrease in 109QmHTT IBs by UbBD mutants. (**A**) Western blot of Neuro2A lysates coexpressing 109QmHTT with WT, truncated or mutated OPTN as indicated. UbBD mutants, 210 to 520Δ, 411 to 520Δ, UbBDΔ, E478G, D474N, increased insolubility index of 109QmHTT, unlike WT or E50K. (B) Western blot of cells coexpressing 109QmHTT with OPTN variant treated with or without 2 μM rapamycin for 24 h. The increased insolubility index by UbBD mutants was not rescued by rapamycin. Corresponding expression of transfected OPTN and mutants was shown in **Fig. S10C** for (**A**) and S10D for (**B**). Asterisks on the blots indicate the insoluble fractions. (**C**) Representative confocal images of Neuro2A cells coexpressing 109QmHTT and OPTN variants acquired by the ImageXpress Micro Imaging XL System. Scale bar: 20 μm. (**D–F**) Quantitative measurements of 109QmHTT IBs in Neuro2A images acquired in (**C**). $^{*}P < 0.05$, $^{***}P < 0.001$, $^{****}P < 0.0001$, ns: not significant. All quantified data were collected from 3 independently performed experiments.

autophagic degradation. To explore the possibility for this change, LC3 turnover (BafA1 over DMSO) under starvation was calculated which revealed that UbBD mutants decreased the LC3 turnover rate; while, WT and E50K increased it (**Fig. 6D**). To validate the specificity of the effect of UbBD mutants, similar experiments were conducted with the LIR mutant F178A, which did not alter the LC3-II level under all tested conditions (**Fig. S6A**). Furthermore, the changes in LC3 levels induced by

Table 1. Percentage of isolated 109QmHTT particles in various fractions

		Ctrl	WT	UbBDΔ	E478G	E50K
P1	Experiment#1	2.7%	↓(1.8%)	↑(3.6%)	↑(3.0%)	↓(1.8%)
	Experiment#2	2.5%	↓(1.7%)	↑(4.0%)	↑(4.4%)	↓(1.7%)
	Experiment#3	3.2%	↓(2.0%)	↑(4.3%)	↑(3.8%)	↓(1.6%)
P5	Experiment#1	1.1%	0.7%	1.3%	1.1%	1.1%
	Experiment#2	0.7%	0.7%	1.4%	1.3%	1.0%
	Experiment#3	0.7%	0.7%	1.3%	1.1%	0.8%
P2	Experiment#1	96.2%	97.5%	95.1%	95.9%	97.1%
	Experiment#2	96.8%	97.6%	94.6%	94.3%	97.3%
	Experiment#3	96.1%	97.3%	94.4%	95.1%	97.6%

The 109QmHTT particles were isolated from Neuro2A cells coexpressing various forms of OPTN as detected by a cell sorter. Three sets of independent experiments are shown here.

WT or OPTN mutants observed above were not caused by corresponding changes in cell survival or *Lc3b* mRNA level (**Fig. S6B to D**). Together, these results demonstrated that WT or E50K overexpression facilitated autophagy, but the UbBD mutants negatively impacted on autophagic flux.

We next examined the effect of UbBD mutants on formation of LC3-positive puncta in MCF7 cells stably expressing GFP-LC3, given its more spread-out cytoplasmic distribution than that seen in Neuro2A cells, in the High Content Image analysis (**Fig. S7**). Under fed conditions, UbBD mutants induced less LC3-positive puncta compared with WT or E50K (**Fig. 6E**). However, under starvation, the number of puncta was lower in cells expressing WT or E50K, but higher in cells expressing UbBD-mutated OPTN (**Fig. 6E**). These data, together with the western blot analyses above, indicated that UbBD-mutated OPTN resulted in impairment in autophagic flux in response to starvation.

We then examined the influence of UbBD mutant OPTN on the level of LC3-II associated with 109QmHTT IBs. As **Fig. 6F** showed, the colocalization of LC3 with 109QmHTT IBs was observed in the presence of WT or OPTN mutants. For further analysis, we isolated the 109QmHTT IBs, and determined the level of LC3-II in them by western blot. The level of LC3-II in the IBs isolated from cells expressing UbBDΔ or E478G was higher than that from control or cells expressing WT or E50K (**Fig. 6G**). Taken together, our data showed that UbBD mutants resulted in accumulation of LC3-II-positive IBs by decreasing autophagy-mediated degradation.

Interference with autophagosome maturation by UbBD mutants

MYO6 has been recently shown to play a role in the fusion of autophagosomes with endosomes by interacting with TOM1.[17] Endogenous MYO6 was found in the isolated 109QmHTT IBs and other OPTN-positive aggregates,[30] but was not associated with 25QHTT (**Fig. S8**). Since MYO6 was previously reported to interact with the region of amino acids 412 to 520 of OPTN,[30] the UbBD-mutant OPTN was hypothesized to affect the autophagosome maturation. Consistent with this notion, immunoprecipitation analysis showed that the E50K mutant interacted with MYO6 as well as WT OPTN, but UbBDΔ or E478G could hardly pull down endogenous MYO6 (**Fig. 7A**). Furthermore, the isolated 109QmHTT IBs contained significantly less MYO6 in the presence of UbBDΔ or E478G compared with WT or E50K (**Fig. 7B**). In addition, the interaction between UbBD-mutant OPTN and the endosome molecule TOM1 was also significantly reduced in comparison with WT or E50K. In 109QmHTT aggregates, the level of TOM1 increased in the presence of WT or E50K, but decreased by UbBDΔ or E478G (**Fig. 7B**). Altogether, these data indicated that the UbBD-mutated OPTN could interfere with the maturation process of autophagy because of reduced capability of recruiting MYO6 during the fusion of autophagosomes with endosomes.

Discussion

Mutations in *OPTN* result in familial cases of primary open-angle glaucoma or ALS. Conventionally viewed as diseases of separate etiology, these 2 types of diseases may share a common pathogenic mechanism in light of the *OPTN* mutations. Accumulated evidence indicates that both glaucoma and ALS can be included under the large umbrella of protein misfolding disease.[31-33] Intriguingly, OPTN has been recently discovered as an important autophagy receptor,[16] and is found in the IBs of a large array of human diseases.[18,20,21,34,35] In this study, we showed that OPTN was also found in the mHTT IBs in HD transgenic mouse models. These lines of evidence raise an interesting possibility that *OPTN* mutations lead to diseases through altering the protein quality control and degradation machinery. Along this, using the *109QmHTT* and *TARDBP*^{ND251} cell models, we demonstrated that WT OPTN indeed decreased the misfolded protein aggregates mainly through polyUbK63-linked autophagy. Moreover, the fact that UbBD mutants disturbed this machinery and the clearance of IBs further substantiated this concept. The recent study by Korac et al. shows that OPTN knockdown increases the IBs,[25] consistent with the data we presented here. In contrast, a decrease in IBs formed by 109QmHTT or TARDBP^{ND251} under overexpression of OPTN was observed in our study, but not by Korac et al. The discrepancy might not be caused by the difference in mHTT protein, and remained to be explained at this time point.

Quite a few mutations in *OPTN* have been discovered in glaucoma and ALS. Alterations in autophagy activity have been proposed as an important mechanism for ALS [36-38] and glaucoma.[39, 40] However, up to now, a unifying mechanism that can satisfactorily explain the pathogenesis of these mutations and diseases remains to be identified. We showed that 210 to 410Δ and E50K whose deletion and mutation were outside the UbBD functioned as the WT OPTN; however, the UbBD mutants such as 210 to 520Δ, 411 to 520Δ, UbBDΔ, E478G, and D474N interfered with the OPTN-mediated degradation of misfolded IBs. These results pointed out that the UbBD not only was a critical region for OPTN function, but also classified disease-associated *OPTN* mutations into 2 mechanistic groups according to the mutation sites in relation to the UbBD. The first group or

UbBD mutants failed to rescue the defect induced by knockdown of OPTN, which was consistent with the previous study.[16] Although they appeared to be dysfunctional or nonfunctional, we further showed that UbBD mutants were more than loss-of-function mutants in that they interfered with autophagic flux through acting as dominant-negative traps for WT OPTN (see below). The second group with disease mutations outside UbBD appeared not to compromise autophagy activity in our study. However, E50K has recently been reported to form misfolded aggregates resulting from an enhanced binding with TBK1,[33] which has been confirmed by another study [41] and our data (**Fig. S9**). Another second group mutant M98K was found to increase autophagy function and caused aberrant degradation of the transferrin receptor.[39] Taken together, it is tempting to hypothesize that mutations in *OPTN* may lead to diseases by tilting the balance of the autophagy activity. More studies are certainly required to further clarify this important issue.

WT OPTN interacts with its polyubiquitinated substrates, which activates TBK1 to phosphorylate OPTN, and enhances subsequent OPTN interaction with LC3 to degrade its substrates through autophagy.[16,17,25,28,42-44] Our data showed that OPTN without UbBD (amino acids 424 to 511) had a significantly reduced ability to bind polyubiquitinated IBs. Korac et al. report that OPTN deleted of the coiled-coil domain (CCD, amino acids 454 to 520) fails to bind IBs.[25] Given the substantial overlapping between UbBD and CCD, our data were considered consistent with those by Korac et al. The finding that UbBD mutants had reduced colocalization with IBs in comparison with WT or non-UbBD mutants also supported

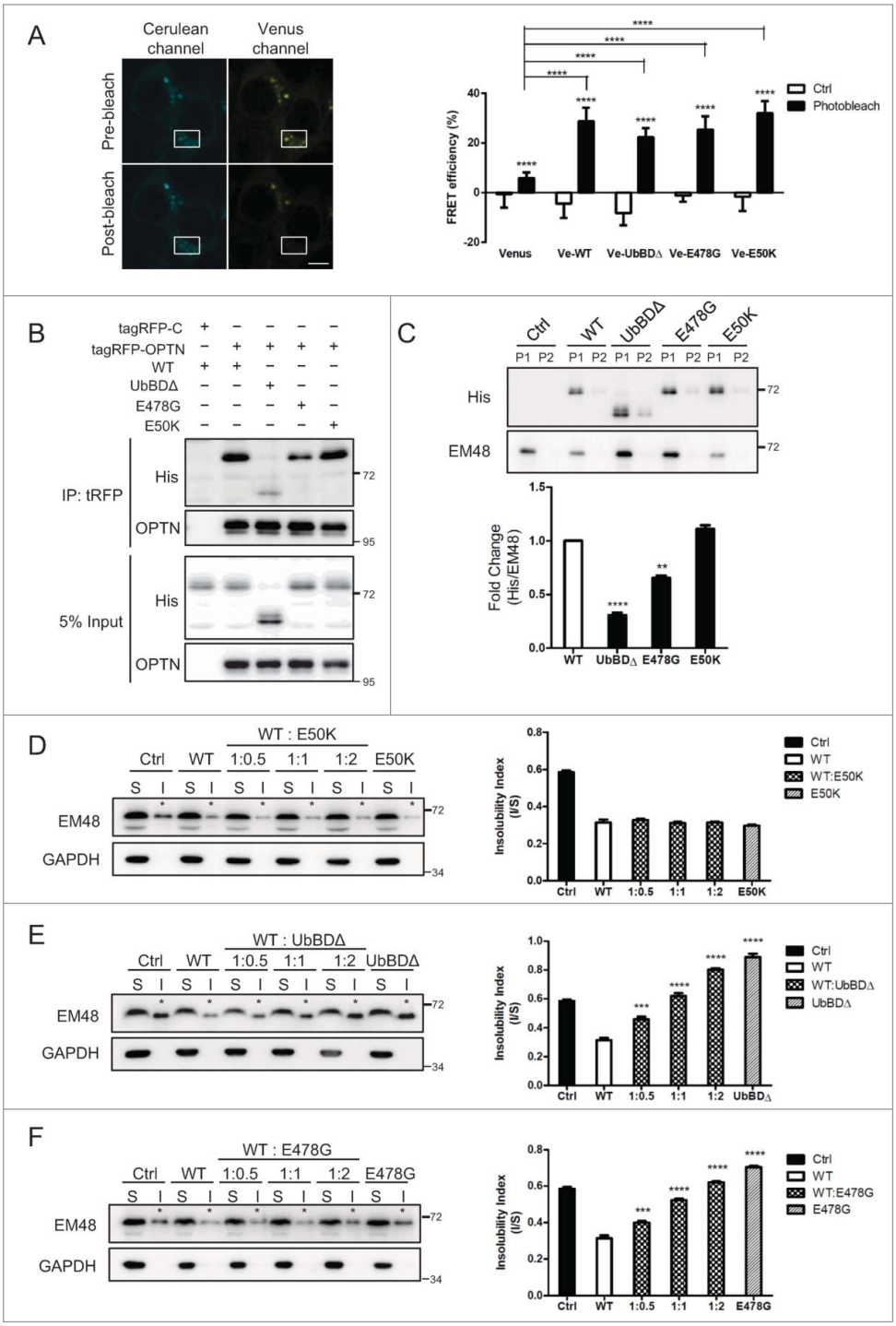

Figure 5. UbBD mutants interacting with WT OPTN and acting as dominant-negative trap. (**A**) Images of Neuro2A cells coexpressing Cerulean-WT OPTN (Ce-WT) and Venus-WT OPTN (Ve-WT) with region of interest (ROI) (boxed) selected for acceptor photobleaching FRET study (Left). Quantification of FRET efficiency of Neuro2A cells coexpression of Ce-WT and Ve-WT or mutant was shown on the right. The same ROI before photobleaching (prebleach) served as Ctrl. (**B**) Interaction of tagRFP-WT OPTN with His-WT OPTN or mutants by immunoprecipitation with anti-tRFP antibody. Immunoblot was done with anti-His (for OPTN variants) and anti-OPTN antibodies. (**C**) Western blot and quantification of the level of WT OPTN and mutants associated with 109QmHTT IBs isolated from Neuro2A cells. The corresponding protein expression is shown in **Figure S10E**. (**D, E, F**) Competition assays in Neuro2A cells showing repression of WT OPTN function by E50K, UbBDΔ or E478G, respectively. The corresponding expression of transfected protein is shown in **Fig. S5**. Asterisks on the blots indicate the insoluble fractions. $^{**}P < 0.01$, $^{***}P < 0.001$, $^{****}P < 0.0001$, ns: not significant. All quantified data were collected from 3 independently performed experiments.

the role of the UbBD CCD in binding OPTN to polyubiquitinated IBs. When put together, these data indicated that the sequence important for IB association could be further shortened to the overlapped region (amino acids 454 to 511).

Counterintuitively, UbBD mutants E478G and D474N, which could not bind polyUb chain,[16,25,42] still retained a solid ability to colocalize with polyubiquitinated IBs in our study (**Fig. 1G**), and also in the study by Korac et al.[25] To solve this

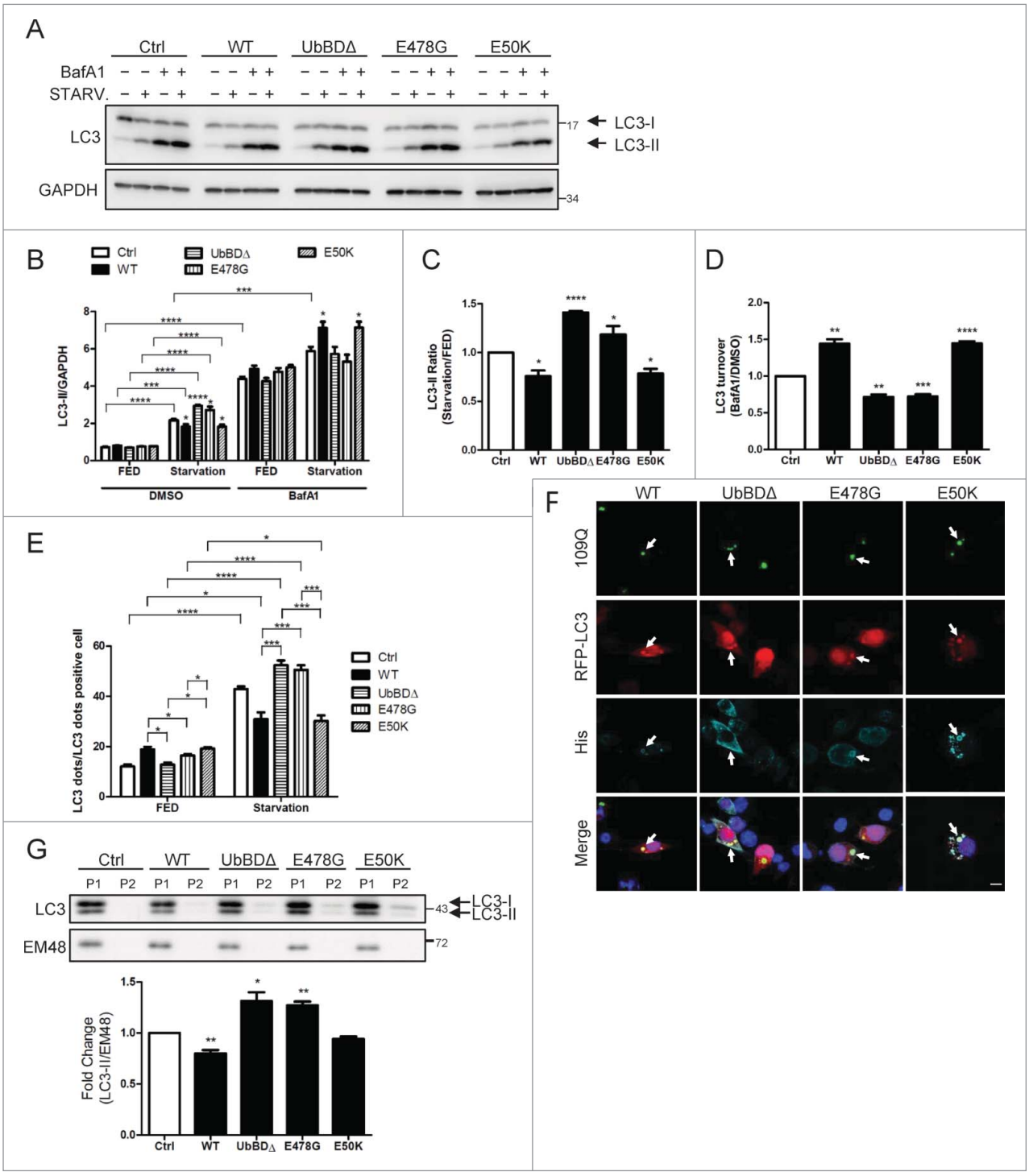

Figure 6. For figure legend, see page 695.

apparent puzzle, Korac et al. hypothesizes an undefined "ubiquitin-independent mechanism" for OPTN-mediated clearance of IBs.[25] OPTN is reported to form hexamers.[29] In this study, we demonstrated using 3 different methods, including confocal imaging, apFRET, and immunoprecipitation, that UbBD mutants interacted with WT OPTN; thus, they could form WT-mutant hybrid OPTN complexes. We proposed that UbBD mutants colocalized with IBs indirectly through the WT partner within the hybrid complex, which was also supported by the finding that showed a lack of association of D477N (mouse equivalent of D474N) with the polyubiquitinated substrate in the homozygous D477N knockin mice, which had no WT OPTN.42 Thus, this interpretation not only was in harmony with the evidence in the previously published studies, but also provided a mechanistic insight into this "ubiquitin-independent" mechanism hypothesized by Korac et al. In conclusion, the UbBD and/or CCD appeared important for WT OPTN's association with IBs; UbBD mutants found in IBs might be indirectly linked through the UbBD and/or CCD of their WT partner in the WT-mutant complex.

In addition, UbBD mutants increased the IBs or insolubility of misfolded proteins as in the case of the OPTN knockdown, and they could repress the function of WT OPTN in clearance of IBs. UbBD mutants were capable of interacting with the WT counterpart, but had lower affinity for partners like MYO6 and TOM1 which were essential for autophagy function. These data indicated that they might well act as dominative-negative traps to compromise the OPTN-mediated autophagy process through formation of WT-mutant complexes. These data suggested that the interference with autophagy-mediated degradation of IBs by UbBD mutants likely happened at 2 steps: 1) association of OPTN with IBs, and 2) autophagosome maturation. Indeed, our data showed that UbBD mutants interfered with autophagic flux (evidenced by alterations in the level and turnover of LC3 and the number of LC3-positive puncta) when cells faced stresses like starvation or formation of IBs where autophagy activity was critically needed. The increased LC3-II level and LC3-positive puncta, but decreased LC3 turnover combined with reduced interaction between the UbBD mutants and MYO6 and TOM1 indicated inhibition of autophagosome fusion with endosomes-lysosomes by UbBD mutants. These changes correlated well with reduced activity in clearance of IBs. These data clearly showed that UbBD mutants decreased clearance of IBs by interfering with OPTN-mediated autophagy. The conclusion is schematically summarized in **Fig. 8**. Recently, increased LC3-II content together with defective clearance of IBs has been recognized as an independent measurement of impairment in autophagic flux, and carries similar significance as a defective LC3 turnover.[45] A recent clinical study hypothesizes that the heterozygous E478G mutation likely causes familial ALS through a dominant-negative mechanism;[46] our current study provided experimental evidence to demonstrate that UbBD mutants indeed act as dominative-negative traps, which may have important clinical implications that may guide development for further therapy of diseases mediated by OPTN dysfunction.

Materials and Methods

Constructs

p*DEST26-hOPTN* (#23050), p*DEST26-hOPTN-D474N* (#23051) and p*mRFP-LC3* (#21075) were purchased from Addgene. Other *OPTN* clones were generated using p*DEST26-hOPTN* as template with primers: 5'CGTGCCAGTG GAGACTGTTC 3' and 5′ACAAGAAAAG AGTCAGAAAA AG3′ for *210 to 410*Δ, 5′CGTGCCAGTG GAGACTGTTC 3′ and 5′CATGGGGCGA GAACAAGTG3′ for *210 to 520*Δ, 5′TAGTTCCTCA ATTGTTTTC3′ and 5′CATGGGGCGA GAACAAGTG3′ for *411 to 520*Δ, 5′CAGTCCTTGA TGGAGATGCA G3′ and 5′CAGCACTGCC CTGTCCACTT 3′ for *UbBD*Δ, 5′AGGATGGCTG AAGGAGAACA G3′ and 5′GGAATCTTCT GAGGAGCCGC T3′ for *LIR*Δ, 5′CAGCGAGAGA GAAAATTCAT G3′ and 5′CTCTTCCAGC ATGAAAATCA G3′ for *E478G*, 5′CTGACCAAGA ACCACCAGCT G3′ and 5′GAGCTCTTTC ATCTGCTGCA G3′ for *E50K*, and 5′CTGTTGAAAT TAGGATGGCT G3′ and 5′CGGAATCTTC TGAGGAGCCG CT3′ for *F178A*. Full-length *OPTN* was subcloned into EcoRI/BamHI sites of the p*TagRFP* vector (a gift from Dr Wei-Yuan Yang, Institute of Biological Chemistry, Academia Sinica). His-tagged *OPTN* and variant constructs were then used as templates with primers 5′AGACTCGAGC ATCACCATCA CCATCACTCT3′ and 5′CTCGGATCCT TAAATGATGC AATCCATCAC3′, then subcloned with NotI/BamHI into p*cDNA3.1-Cerulean* or p*cDNA3.1-Venus* (gift of Dr C Y Tai, Institute of Molecular Biology, Academia Sinica).[47] p*eGFP-TARDBP*^{ND251} (p*eGFP-TARDBP*^{ND251}), p*eGFP-HTT25Q* and p*eGFP-HTT109Q* (exon1) were previously described.[26,48,49]

Figure 6 (See previous page). Decreased autophagic flux by UbBD mutants. (**A**) Western blot and (**B**) corresponding quantification of LC3-II in Neuro2A cells expressing WT or mutant OPTN under fed (starvation-) or starvation (+) conditions, treated with DMSO (−) or BafA1, as indicated. The corresponding protein expression is shown in **Fig. S10F**. LC3-II expression was normalized against GAPDH. (**C**) Quantitative data on the effect of UbBD mutants on the fold change in LC3-II in response to starvation. The fold change was first calculated with the value of each sample in the starvation with DMSO group divided by corresponding sample in FED with DMSO group, which were then normalized with the Ctrl (set as 1). (**D**) Effect of UBbD mutants on LC3 turnover. Quantitative data were first calculated with the value of each sample in the starvation plus BafA1 group divided by corresponding sample in the starvation plus DMSO groups, which were then normalized with the Ctrl (set as 1). (**E**) Effect of the UbBD mutants on the number of GFP-LC3 dots from the images acquired by the ImageXpress Micro Imaging XL System (**Fig. S7**) with the indicated conditions on MCF7 cells stably expressing GFP-LC3. The corresponding protein expression was shown in **Figure S10G**. (**F**) Colocalization of WT and the mutant OPTN shown in confocal micrographs of Neuro2A cells co-overexpressing 109QmHTT, RFP-LC3 plus WT or mutant OPTN as indicated. Scale bar: 5 μm. (**G**) Western blot analysis of the RFP-LC3-II level in the isolated 109QmHTT IBs (P1) or soluble fraction (P2) from cells coexpressing WT or mutant OPTN as indicated (upper panel). Notably, LC3 was highly enriched in IB fraction. Quantitfication of the LC3-II level was shown in lower panel. Corresponding protein expression is shown in **Fig. S10H**. *$P < 0.05$, **$P < 0.01$, ***$P < 0.001$, ****$P < 0.0001$. All quantified data were collected from 3 independently performed experiments.

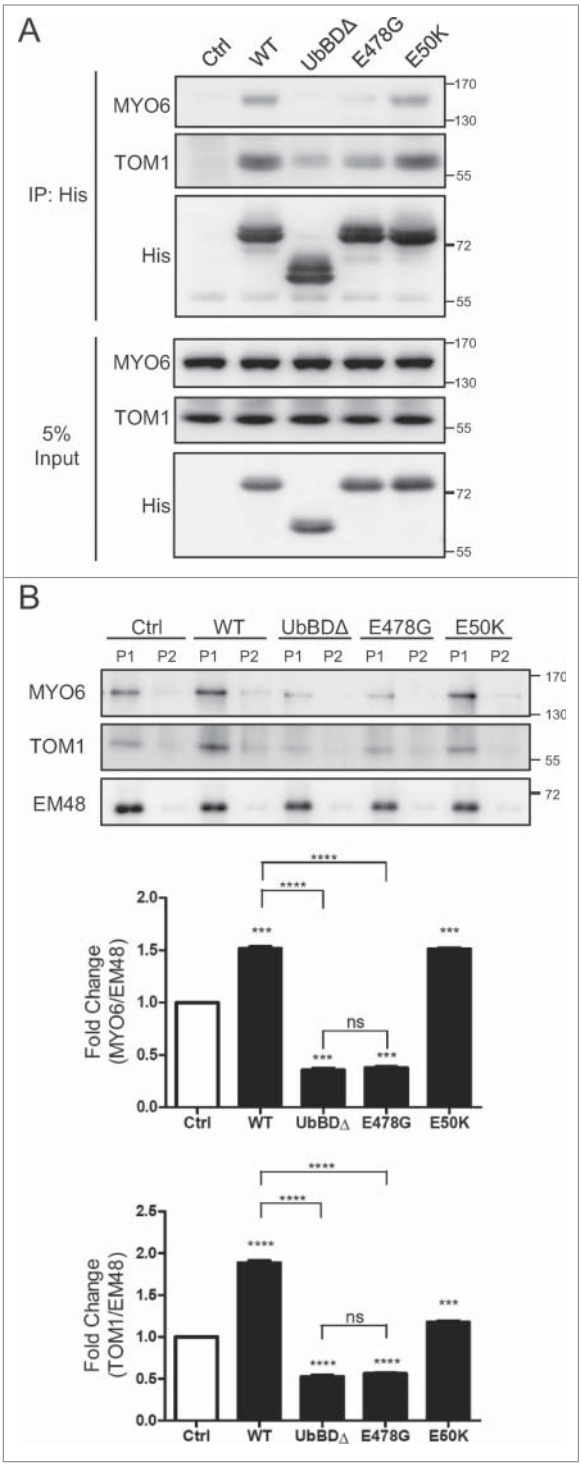

Figure 7. Reduced interaction between MYO6 and UbBD mutants. (**A**) MYO6 and TOM1 was pulled down from cells expressing His-WT or mutant OPTN as indicated with Ni-Sepharose™ beads. Cells were treated with 200 nM BafA1 for 16 h before harvest. Western blots were performed with antibodies as indicated in IP panel. (**B**) The level of MYO6 and TOM1 associated with the sorted 109QmHTT IBs from Neuro2A cells coexpressing WT or mutant OPTN. Corresponding protein expression is shown in **Fig. S10E**. ***$P < 0.001$, ****$P < 0.0001$, ns: not significant. All quantified data were collected from 3 independently performed experiments.

p*eGFP-HTT25QN* and p*eGFP-HTT81QN* were made with primers 5′CGAAAGGTGG GTGATATCCA GCACAGTGGC GGCC3′ and 5′CTTCTTCTTC GGTGCAGAAT TGCC-CTTTCG GTGC3′ to insert the SV40 nuclear localization signal (NLS) into the p*eGFP-Htt25Q* and p*eGFP-Htt109Q* templates. p*cDNA3.1-His-Ubiquitin*, p*cDNA3.1-His-UbK48R* and p*cDNA3.1-His-UbK63R* were kindly provided by Dr Ruey-Hwa Chen (Institute of Biological Chemistry, Academia Sinica).

Antibodies and reagents

Antibodies used in this study included OPTN (C-Term, 100000, Cayman); HTT (clone mEM48, MAB5374, Millipore); His (clone HIS.H8, 05-949, Millipore); GAPDH (MAB374, Millipore); GFP (A11122, Invitrogen); TUBA/alpha tubulin (clone B-5-1-2, T5168, Sigma); ATG5 (GTX62601, GeneTex); tRFP (AB233, Evrogen); Ub (Z0458, Dako Cytomation); UbK48-Specific (clone Apu2, 05-1307, Millipore); UbK63-specific (clone HWA4C4, 05-1313, Millipore); MYO6 (ABT42, Millipore); TOM1L2 (ab96320, Abcam); LC3 (PM036, MBL). Peroxidase- or DyLight™ 488-conjugated secondary antibodies were from Jackson ImmunoResearch (115-035-146; 111-035-003; 715-485-151; 711-485-152); AlexaFluor 546- and Cy5-labled secondary antibodies were from Invitrogen (A11030; A11035; A10524; A10523). Reagents used were MG-132 (474790, Calbiochem); 3-methyladenine (M9281, Sigma); bafilomycin A_1 (B1793, Sigma); rapamycin (#553210, Calbiochem).

Cell preparation and transfection of siRNA and polyubiquitin chains

HEK293T, Neuro2A cell lines (CRL-11268 and CCL-131, American Type Culture Collection) and MEF as well as MEF *atg5*$^{-/-}$ cell lines (gift of Dr Noboru Mizushima, Department of Biochemistry and Molecular Biology, The University of Tokyo) were propagated in DMEM (Gibco, 12800-017) with 10% fetal bovine serum and 1% penicillin-streptomycin (Gibco, 15140-122). 1×10^5 and 5×10^5 Neuro2A cells were plated on coverslips and in 6-well plates for immunofluorescence staining and protein extraction, respectively. Cells were transfected by using Lipofectamine 2000 (Invitrogen, 11668-500) or Maestrofectin (Omics Bio, MF002) for specified times or 30 h. *Optn* shRNA was purchased from the National RNAi Core Facility Platform (Academia Sinica, Taiwan). *Atg5* Stealth siRNA and Stealth RNAi Negative Control Duplex were purchased from Invitrogen and transfected into cells using Lipofectamin RNAiMAX (Invitrogen, 13778-075). For polyUb chains transfection, Neuro2A cells were first transfected with e*GFP-Htt109Q* as well as the control or *OPTN* plasmids 6 h ahead. polyUbK48 or polyUbK63 chains (#UC-240 and #UC-340, BostonBiochem) were then transfected into cells using PULSin™ Protein delivery reagent (501-04, PolyPlus) following the manufacturer's suggestions.

Immunofluorescence staining

The transfected cells on coverslips were fixed with 4% paraformaldehyde/phosphate-buffered saline (PFA/PBS; 137 mM NaCl, 2.7 mM KCl, 10 mM Na_2HPO_4, 1.8 mM KH_2PO_4) for 15 min and then permeabilized with 0.2% Triton X-100

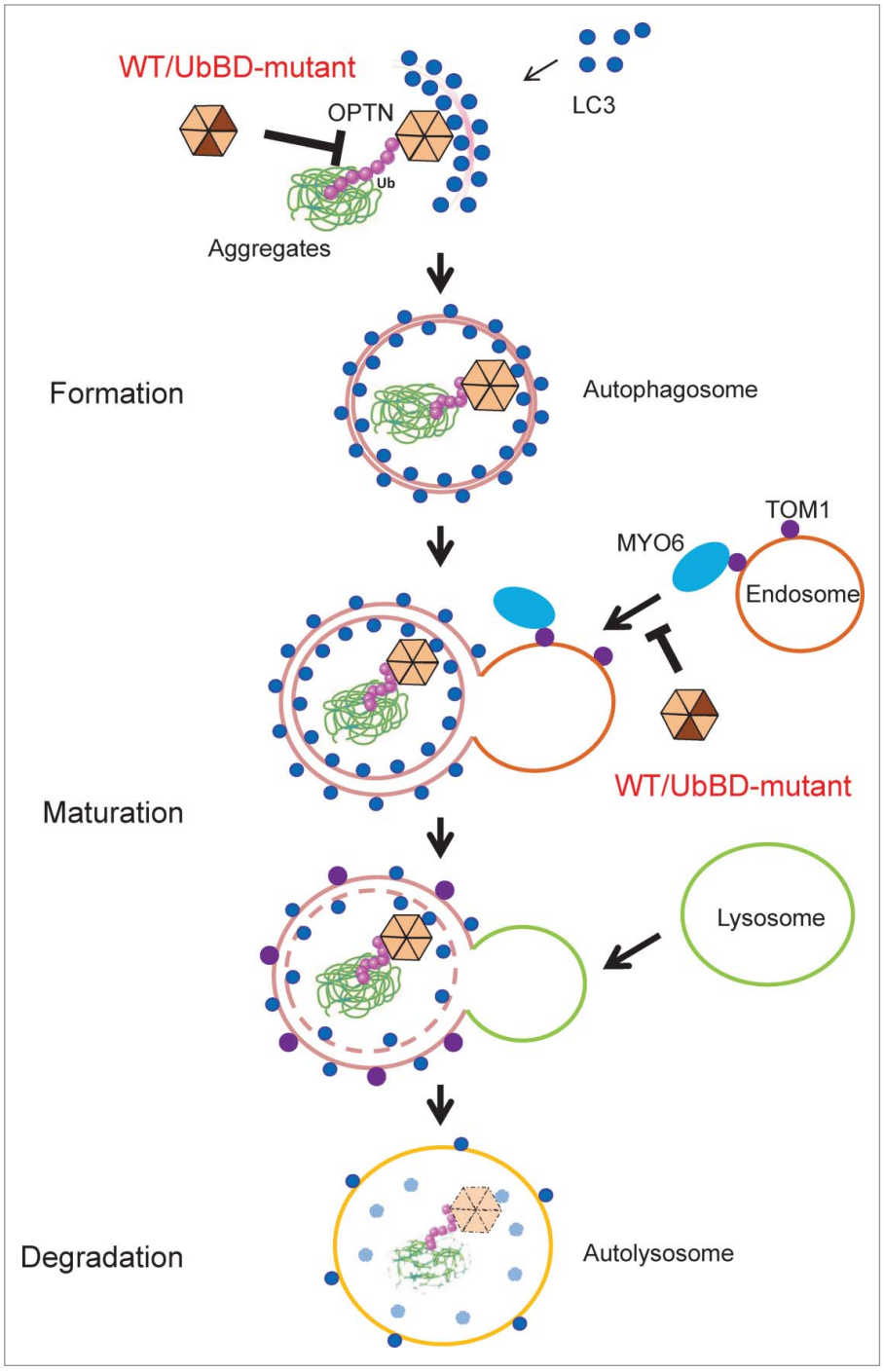

Figure 8. The schematic model of UbBD mutants as dominant-negative traps to interfere with autophagy-mediated IB degradation. UbBD-mutants interacted with the WT counterpart, and formed an WT-mutant hybrid oligomer or complex. Given their weaker affinity with IBs, MYO6, and TOM1, they decreased autophagy flux at both early and late stages and subsequent degradation of IBs.

(PlusOne, 45-000-229)/PBS for 10 min. appropriate diluted primary antibodies and fluorescently-labeled secondary antibodies in 2% bovine serum albumin (Sigma, A7906)/PBS were covered on the coverslips at 4°C over 2 nights and overnight, respectively. Nuclei were counterstained with DAPI for 10 min. Images were taken by LSM510 META confocal microscope (Carl Zeiss, Göttingen, Germany)

Analyses of IBs with high content images

For high content image analysis, 1×10^5 Neuro2A cells were plated on 24-well plates (Costar 3524, Corning Inc.), and fixed with 4% PFA/PBS for 15 min 30 h post transfection. After 10 min penetration with 0.2% Triton X-100/PBS and following 10 min staining with DAPI, cells were preserved in PBS. Images were taken and analyzed by ImageXpress Micro Imaging XL System (Molecular Devices, Sunnyvale, CA, USA).

Analysis of isolated IBs

Isolation of mHTT and TARDBP^{ND251} IBs with a FACSAria cell sorter was conducted as previously described,[26] and shown in **Fig. S1**. But the lysis buffer for mHTT IBs was slightly modified to 20 mM Tris-HCl, pH 7.5, 150 mM NaCl, 1 mM EDTA, 1% Triton X-100, 0.25% SDS (JT Baker, 4095-02) with protease inhibitor (Roche, 05892791001).

Analyses of acceptor photobleaching FRET

Ce-OPTN and *Ve-OPTN* or mutant constructs were cotransfected into Neuro2A cells for 48 h and then fixed with 4% PFA/PBS for 15 min. Images were taken using an LSM510 META confocal microscope (Carl Zeiss) with a previously described protocol.[50] In brief, a series of images were taken before, during, and after photobleaching with 458 nm and 514 nm laser. The Venus signal was bleached by 100% 514 nm laser in the region of interest (ROI). The efficiency of FRET was analyzed with the end time point (210 sec) by ZEN 2011 Imaging Software (Carl Zeiss). The region without photobleaching in each image was used as control. At least 50 ROIs were analyzed from more than 10 cells in each experimental group.

Analyses of GFP-LC3 puncta

The MCF7-GFP-LC3 stable line (gift of Noboru Mizushima) was cultured in DMEM with 10% fetal bovine serum, 1% penicillin-streptomycin and 2 mg/ml G418 (Sigma, A1720). After 8 h transfection, transfected MCF7-GFP-LC3 cells were subcultured on 96-well plates (CellCarrier-96, 6005550, PerKin)

overnight. Completed medium was change into all groups of experiment cells one h ahead of starvation. For starvation condition, EBSS (Sigma, E3024) was used for 2.5 h after PBS washed once. For high content image analysis, cells were fixed after starvation and stained with DAPI as aforementioned. Images were taken and analyzed by ImageXpress Micro Imaging XL System (Molecular Devices). Additional criteria for analysis were: for LC3 dots, GFP intensity must be higher than 5000 and for LC3 dot-positive cells, the numbers of LC3 dots need to be more than 15.

Filter-trap analysis

Samples were prepared with ice-cold RIPA buffer as previously described.[26] Briefly, 30 μg of total protein lysate was loaded onto one well of 0.2 μm cellulose acetate membrane (C020A293C, ADVANTEC). After rinsing with RIPA buffer, the cellulose acetate membrane was removed from Dot Blotter Unit (MDHM-48, Major Science) and GFP signals were detected with a Typhoon9410 Variable Mode Imager (Amersham BioSciences, Piscataway, NJ, USA)

Fractionation and insolubility assay

For insolubility assay, the sample was extracted twice with RIPA buffer, each followed by sonication and centrifugation at 16,000 × g, 4°C for 10 min. The supernatant of first extraction was saved as the RIPA-soluble (S) fraction. The pellet was then resuspended and sonicated in buffer with 2% SDS/6 M urea (BioShop, URE002) as RIPA-insoluble (I) fraction. The loading volume for each sample was first adjusted by the GAPDH signal in the S fraction to make sure equal loading across samples. Then, each pair of the S and I fraction of the same sample was loaded proportionally, and the final signal of protein of interest was normalized with GAPDH in the adjusted sample. The insolubility index was calculated as the ratio of signal in I fraction/signal in the S fraction (insolubility index).

LC3 turnover assay

Neuro2A cells were transfected with various *OPTN* constructs as indicated, for 48 h. Serum-free medium was replaced for starvation 24 h after transfection, and cells were treated with 1 μM DMSO or BafA1 16 h before harvest, respectively. The expression of LC3-II level was quantified with an ImageQuantTL system (Molecular Devices) and then normalized with the expression of GAPDH.

Cell viability and real-time PCR

Neuro2A cells were treated as the MCF7-GFP-LC3 cells described above. Cell viability was performed with PrestoBlue™ Cell Viability Reagent (Invitrogen, A13261), total RNA was extracted with TRIzol® (Invitrogen, 15596-018) and cDNA was synthesized with SuperScript® III Reverse Transcriptase (Invitrogen, 18080-044) following the manufacturers' suggestions. Real-time quantitative PCR was performed and analyzed using SYBR® *Premix Ex* Tag™ (RR420A, TaKaRa) and a 7500 Real-Time PCR System (Applied Biosystems, Foster City, CA, USA). The amplification primers were 5′CGTCCTGGAC AAGACCAAGT 3′ and 5′ATTGCTGTCC CGAATGTCTC 3′ for *Lc3b*, and 5′ GGAGCCAAAC GGGTCATCAT CTC3′ and 5′ GAGGGGCCAT CCACAGTCTT CT3′ for *Gapdh*. The *Lc3b* mRNA levels were normalized with *Gapdh*.

Immunoprecipitation

Neuro2A cells were lysed 48 h after transfection with IP buffer (20 mM Tris-HCl, pH 8.0, 137 mM NaCl, 10% glycerol, 2 mM EDTA, 0.2% Triton X-100 and complete protease inhibitor) on ice for 30 min with shaking, centrifuged at 16,000 × g for 10 min, and then supernatant were precleaned for 1 h by with Protein G Sepharose™ (17-0618-01, GE Healthcare) on a shaker at 4°C. 2 mg precleaned lysate were incubated with 2.5 μg tRFP antibody for 2 h at 4°C and then 25 μl Protein G Sepharose™ were added into the mixture with overnight incubation on a shaker at 4°C. The incubated beads were centrifuged and washed 5 times with IP lysis buffer. 100 μl 2x sample buffer (100 mM Tris-HCl, pH 6.8, 4% SDS, 20% glycerol, 10% β-mercaptoethanol, 0.05% bromophenol blue) were added with the washed beads and then resolved by SDS-PAGE for immunoblotting. Endogenous MYO6 and TOM1 immunopricipitation was performed according to a previous description.[51] In brief, HEK293T cells were lysed with 1x PBS containing 1 mM EDTA, 5 mM ATP, 5 mM $MgCl_2$, 0.5% NP-40 (usb, 19628) and complete protease inhibitor. After sonication and centrifugation, 5 mg cell lysate were incubated with 30 μl Ni Sepharose™ (17-5318-01, GE Healthcare) overnight at 4°C. The beads were then washed with the same lysis buffer 8 times and subjected to SDS-PAGE fractionation for following immunoblotting.

Transgenic mice and tissue preparation

R6/2 transgenic mice[11] and female control breeders (B6CBAFI/J) were obtained from Jackson Laboratories (Bar Harbor, ME, USA). The offspring was genotyped by polymerase chain reaction (PCR) with primers 5′CCGCTCAGGT TCTGCTTTTA 3′ and 5′GGCTGAGGAA GCTGAGGAG3′. The numbers of the CAG repeats of R6/2 mice were 250 to 270. Animals were housed at the Institute of Biomedical Sciences Animal Care Facility. Animal experiments were performed under protocols approved by the Academia Sinica Institutional Animal Care and Utilization Committee, Taiwan. Mice were sacrificed by suffocation and their brains were fixed with 4% PFA/PBS and subsequently prepared as paraffin-embedded sections. For immunohistofluorescent staining, brain sections were deparaffinized and rehydrated before being boiled with 10% sodium citrate, pH 6.0/0.05% Tween 20 for 30 min. After being blocked in 5% H_2O_2/methanol for 30 min and 2% bovine serum albumin/PBS for 1 h, sections were covered with the first primary antibody diluted in blocking buffer overnight, and the appropriate secondary antibody for 2 h; the sections were then stained with a second primary antibody and processed as mentioned with nuclear counterstain with 0.1 μg/ml DAPI/PBS for 10 min before mounting. Fluorescent images were taken with an LSM510 META confocal microscope.

Statistics

Quantifications in this study were analyzed with the Student *t* test, one-way ANOVA or 2-way ANOVA for 2, 3, or more groups with a single variable or groups with more than one variable, respectively, using GraphPad Prism 5 (GraphPad Software, Inc.). The Bonferroni multiple comparison was used following the ANOVA as post-hoc analysis.

Disclosure of Potential Conflicts of Interest

No potential conflicts of interest were disclosed.

Acknowledgements

The authors thank the staff of the common facility and pathology core of the Institute of Biomedical Sciences, Academia Sinica (AS), for their excellent technical support; Dr Ruey-Hwa Chen and Dr Wei-Yuan Yang, Institute of Biological Chemistry, AS, and Dr C Y Tai, Institute of Molecular Biology, AS. for sharing constructs; Dr Noboru Mizushima, Department of Biochemistry and Molecular Biology, The University of Tokyo, for sharing cells as described in Materials and Methods. The shRNAs were obtained from the National RNAi Core of Taiwan, Institute of Molecular Biology, AS.

Funding

The project was funded by the AS.

Supplemental Material

Supplemental data for this article can be accessed on the publisher's website.

References

1. Ross CA, Poirier MA. Protein aggregation and neurodegenerative disease. Nature medicine 2004; 10 Suppl: S10-7.
2. Neumann M, Sampathu DM, Kwong LK, Truax AC, Micsenyi MC, Chou TT, et al. Ubiquitinated TDP-43 in frontotemporal lobar degeneration and amyotrophic lateral sclerosis. Science 2006; 314:130-3.
3. Arai T, Hasegawa M, Akiyama H, Ikeda K, Nonaka T, Mori H, et al. TDP-43 is a component of ubiquitin-positive tau-negative inclusions in frontotemporal lobar degeneration and amyotrophic lateral sclerosis. Biochemical and biophysical research communications 2006; 351:602-11.
4. Ince PG, Highley JR, Kirby J, Wharton SB, Takahashi H, Strong MJ, et al. Molecular pathology and genetic advances in amyotrophic lateral sclerosis: an emerging molecular pathway and the significance of glial pathology. Acta neuropathologica 2011; 122:657-71.
5. Clague MJ, Urbe S. Ubiquitin: same molecule, different degradation pathways. Cell 2010; 143:682-5.
6. Cheong H, Klionsky DJ. Dual role of Atg1 in regulation of autophagy-specific PAS assembly in Saccharomyces cerevisiae. Autophagy 2008; 4:724-6.
7. Kraft C, Peter M, Hofmann K. Selective autophagy: ubiquitin-mediated recognition and beyond. Nature cell biology 2010; 12:836-41.
8. Kirkin V, McEwan DG, Novak I, Dikic I. A role for ubiquitin in selective autophagy. Molecular cell 2009; 34:259-69.
9. Pankiv S, Clausen TH, Lamark T, Brech A, Bruun JA, Outzen H, et al. p62/SQSTM1 binds directly to Atg8/LC3 to facilitate degradation of ubiquitinated protein aggregates by autophagy. The Journal of biological chemistry 2007; 282:24131-45.
10. Kirkin V, Lamark T, Sou YS, Bjorkoy G, Nunn JL, Bruun JA, et al. A role for NBR1 in autophagosomal degradation of ubiquitinated substrates. Molecular cell 2009; 33:505-16.
11. Thurston TL, Ryzhakov G, Bloor S, von Muhlinen N, Randow F. The TBK1 adaptor and autophagy receptor NDP52 restricts the proliferation of ubiquitin-coated bacteria. Nature immunology 2009; 10:1215-21.
12. Paine S, Bedford L, Thorpe JR, Mayer RJ, Cavey JR, Bajaj N, et al. Immunoreactivity to Lys63-linked polyubiquitin is a feature of neurodegeneration. Neuroscience letters 2009; 460:205-8.
13. Lim KL, Lim GG. K63-linked ubiquitination and neurodegeneration. Neurobiology of disease 2011; 43:9-16.
14. Tan JM, Wong ES, Kirkpatrick DS, Pletnikova O, Ko HS, Tay SP, et al. Lysine 63-linked ubiquitination promotes the formation and autophagic clearance of protein inclusions associated with neurodegenerative diseases. Human molecular genetics 2008; 17:431-9.
15. Ramsey WJ, Caplen NJ, Li Q, Higginbotham JN, Shah M, Blaese RM. Adenovirus vectors as transcomplementing templates for the production of replication defective retroviral vectors. Biochemical and biophysical research communications 1998; 246:912-9.
16. Wild P, Farhan H, McEwan DG, Wagner S, Rogov VV, Brady NR, et al. Phosphorylation of the autophagy receptor optineurin restricts Salmonella growth. Science 2011; 333:228-33.
17. Tumbarello DA, Waxse BJ, Arden SD, Bright NA, Kendrick-Jones J, Buss F. Autophagy receptors link myosin VI to autophagosomes to mediate Tom1-dependent autophagosome maturation and fusion with the lysosome. Nature cell biology 2012; 14:1024-35.
18. Maruyama H, Morino H, Ito H, Izumi Y, Kato H, Watanabe Y, et al. Mutations of optineurin in amyotrophic lateral sclerosis. Nature 2010; 465:223-6.
19. Schwab C, Yu S, McGeer EG, McGeer PL. Optineurin in Huntington's disease intranuclear inclusions. Neuroscience letters 2012; 506:149-54.
20. Mori F, Tanji K, Toyoshima Y, Yoshida M, Kakita A, Takahashi H, et al. Optineurin immunoreactivity in neuronal nuclear inclusions of polyglutamine diseases (Huntington's, DRPLA, SCA2, SCA3) and intranuclear inclusion body disease. Acta neuropathologica 2012; 123:747-9.
21. Osawa T, Mizuno Y, Fujita Y, Takatama M, Nakazato Y, Okamoto K. Optineurin in neurodegenerative diseases. Neuropathology : official journal of the Japanese Society of Neuropathology 2011; 31:569-74.
22. Okita S, Morigaki R, Koizumi H, Kaji R, Nagahiro S, Goto S. Cell type-specific localization of optineurin in the striatal neurons of mice: implications for neuronal vulnerability in Huntington's disease. Neuroscience 2012; 202:363-70.
23. Anborgh PH, Godin C, Pampillo M, Dhami GK, Dale LB, Cregan SP, et al. Inhibition of metabotropic glutamate receptor signaling by the huntingtin-binding protein optineurin. The Journal of biological chemistry 2005; 280:34840-8.
24. De Marco N, Buono M, Troise F, Diez-Roux G. Optineurin increases cell survival and translocates to the nucleus in a Rab8-dependent manner upon an apoptotic stimulus. The Journal of biological chemistry 2006; 281:16147-56.
25. Korac J, Schaeffer V, Kovacevic I, Clement AM, Jungblut B, Behl C, et al. Ubiquitin-independent function of optineurin in autophagic clearance of protein aggregates. Journal of cell science 2013; 126:580-92.
26. Li HY, Yeh PA, Chiu HC, Tang CY, Tu BP. Hyperphosphorylation as a defense mechanism to reduce TDP-43 aggregation. PloS one 2011; 6:e23075.
27. Urry DW, Harris RD, Long MM, Prasad KU. Polytetrapeptide of elastin. Temperature-correlated elastomeric force and structure development. International journal of peptide and protein research 1986; 28:649-60.
28. Nagabhushana A, Chalasani ML, Jain N, Radha V, Rangaraj N, Balasubramanian D, et al. Regulation of endocytic trafficking of transferrin receptor by optineurin and its impairment by a glaucoma-associated mutant. BMC cell biology 2010; 11:4.
29. Ying H, Shen X, Park B, Yue BY. Posttranslational modifications, localization, and protein interactions of optineurin, the product of a glaucoma gene. PloS one 2010; 5:e9168.
30. Sahlender DA, Roberts RC, Arden SD, Spudich G, Taylor MJ, Luzio JP, et al. Optineurin links myosin VI to the Golgi complex and is involved in Golgi organization and exocytosis. The Journal of cell biology 2005; 169:285-95.
31. Burns JN, Turnage KC, Walker CA, Lieberman RL. The stability of myocilin olfactomedin domain variants provides new insight into glaucoma as a protein misfolding disorder. Biochemistry 2011; 50:5824-33.
32. Ghiso JA. Alzheimer's disease and glaucoma: mechanistic similarities and differences. Journal of glaucoma 2013; 22 Suppl 5:S36-8.
33. Minegishi Y, Iejima D, Kobayashi H, Chi ZL, Kawase K, Yamamoto T, et al. Enhanced optineurin E50K-TBK1 interaction evokes protein insolubility and initiates familial primary open-angle glaucoma. Human molecular genetics 2013.
34. Hortobagyi T, Troakes C, Nishimura AL, Vance C, van Swieten JC, Seelaar H, et al. Optineurin inclusions occur in a minority of TDP-43 positive ALS and FTLD-TDP cases and are rarely observed in other neurodegenerative disorders. Acta neuropathologica 2011; 121:519-27.
35. Schwab C, Yu S, McGeer PL. Optineurin is colocalized with ubiquitin in Marinesco bodies. Acta neuropathologica 2012; 123:289-92.
36. Filimonenko M, Stuffers S, Raiborg C, Yamamoto A, Malerod L, Fisher EM, et al. Functional multivesicular bodies are required for autophagic clearance of protein aggregates associated with neurodegenerative disease. The Journal of cell biology 2007; 179:485-500.
37. Pasquali L, Ruffoli R, Fulceri F, Pietracupa S, Siciliano G, Paparelli A, et al. The role of autophagy: what can be learned from the genetic forms of amyotrophic lateral sclerosis. CNS & neurological disorders drug targets 2010; 9:268-78.
38. Castillo K, Nassif M, Valenzuela V, Rojas F, Matus S, Mercado G, et al. Trehalose delays the progression of amyotrophic lateral sclerosis by enhancing autophagy in motoneurons. Autophagy 2013; 9.
39. Sirohi K, Chalasani ML, Sudhakar C, Kumari A, Radha V, Swarup G. M98K-OPTN induces transferrin receptor

degradation and RAB12-mediated autophagic death in retinal ganglion cells. Autophagy 2013; 9:510-27.
40. Park HY, Kim JH, Park CK. Activation of autophagy induces retinal ganglion cell death in a chronic hypertensive glaucoma model. Cell death & disease 2012; 3: e290.
41. Morton S, Hesson L, Peggie M, Cohen P. Enhanced binding of TBK1 by an optineurin mutant that causes a familial form of primary open angle glaucoma. FEBS letters 2008; 582:997-1002.
42. Gleason CE, Ordureau A, Gourlay R, Arthur JS, Cohen P. Polyubiquitin binding to optineurin is required for optimal activation of TANK-binding kinase 1 and production of interferon beta. The Journal of biological chemistry 2011; 286:35663-74.
43. Zhu G, Wu CJ, Zhao Y, Ashwell JD. Optineurin negatively regulates TNFalpha- induced NF-kappaB activation by competing with NEMO for ubiquitinated RIP. Current biology : CB 2007; 17:1438-43.
44. Laplantine E, Fontan E, Chiaravalli J, Lopez T, Lakisic G, Veron M, et al. NEMO specifically recognizes K63-linked poly-ubiquitin chains through a new bipartite ubiquitin-binding domain. The EMBO journal 2009; 28:2885-95.
45. Klionsky DJ, Abeliovich H, Agostinis P, Agrawal DK, Aliev G, Askew DS, et al. Guidelines for the use and interpretation of assays for monitoring autophagy in higher eukaryotes. Autophagy 2008; 4:151-75.
46. Ito H, Nakamura M, Komure O, Ayaki T, Wate R, Maruyama H, et al. Clinicopathologic study on an ALS family with a heterozygous E478G optineurin mutation. Acta neuropathologica 2011; 122:223-9.
47. Kim SA, Tai CY, Mok LP, Mosser EA, Schuman EM. Calcium-dependent dynamics of cadherin interactions at cell-cell junctions. Proceedings of the National Academy of Sciences of the United States of America 2011; 108:9857-62.
48. Cao Y, Klionsky DJ. New insights into autophagy using a multiple knockout strain. Autophagy 2008; 4:1073-5.
49. Chiang MC, Chen HM, Lee YH, Chang HH, Wu YC, Soong BW, et al. Dysregulation of C/EBPalpha by mutant Huntingtin causes the urea cycle deficiency in Huntington's disease. Human molecular genetics 2007; 16:483-98.
50. Karpova T, McNally JG. Detecting protein-protein interactions with CFP-YFP FRET by acceptor photobleaching. Current protocols in cytometry / editorial board, J Paul Robinson, managing editor [et al] 2006; Chapter 12: Unit12 7.
51. Buss F, Kendrick-Jones J, Lionne C, Knight AE, Cote GP, Paul Luzio J. The localization of myosin VI at the golgi complex and leading edge of fibroblasts and its phosphorylation and recruitment into membrane ruffles of A431 cells after growth factor stimulation. The Journal of cell biology 1998; 143:1535-45.